NIST SPECIAL PUBLICATION 400-95

U.S. DEPARTMENT OF COMMERCE/Technology Administration
National Institute of Standards and Technology

Semiconductor Measurement Technology:

User's Manual for the Program MONSEL-1: Monte Carlo Simulation of SEM Signals for Linewidth Metrology

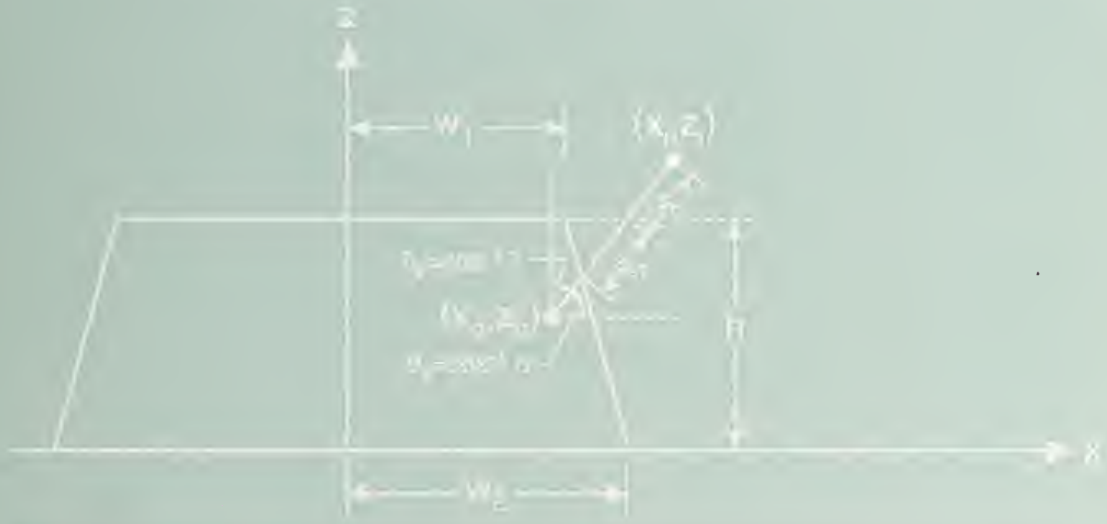

J. R. Lowney and P. Marx

The National Institute of Standards and Technology was established in 1988 by Congress to "assist industry in the development of technology . . . needed to improve product quality, to modernize manufacturing processes, to ensure product reliability . . . and to facilitate rapid commercialization . . . of products based on new scientific discoveries."

NIST, originally founded as the National Bureau of Standards in 1901, works to strengthen U.S. industry's competitiveness; advance science and engineering; and improve public health, safety, and the environment. One of the agency's basic functions is to develop, maintain, and retain custody of the national standards of measurement, and provide the means and methods for comparing standards used in science, engineering, manufacturing, commerce, industry, and education with the standards adopted or recognized by the Federal Government.

As an agency of the U.S. Commerce Department's Technology Administration, NIST conducts basic and applied research in the physical sciences and engineering and performs related services. The Institute does generic and precompetitive work on new and advanced technologies. NIST's research facilities are located at Gaithersburg, MD 20899, and at Boulder, CO 80303. Major technical operating units and their principal activities are listed below. For more information contact the Public Inquiries Desk, 301-975-3058.

Technology Services
- Manufacturing Technology Centers Program
- Standards Services
- Technology Commercialization
- Measurement Services
- Technology Evaluation and Assessment
- Information Services

Electronics and Electrical Engineering Laboratory
- Microelectronics
- Law Enforcement Standards
- Electricity
- Semiconductor Electronics
- Electromagnetic Fields[1]
- Electromagnetic Technology[1]

Chemical Science and Technology Laboratory
- Biotechnology
- Chemical Engineering[1]
- Chemical Kinetics and Thermodynamics
- Inorganic Analytical Research
- Organic Analytical Research
- Process Measurements
- Surface and Microanalysis Science
- Thermophysics[2]

Physics Laboratory
- Electron and Optical Physics
- Atomic Physics
- Molecular Physics
- Radiometric Physics
- Quantum Metrology
- Ionizing Radiation
- Time and Frequency[1]
- Quantum Physics[1]

Manufacturing Engineering Laboratory
- Precision Engineering
- Automated Production Technology
- Robot Systems
- Factory Automation
- Fabrication Technology

Materials Science and Engineering Laboratory
- Intelligent Processing of Materials
- Ceramics
- Materials Reliability[1]
- Polymers
- Metallurgy
- Reactor Radiation

Building and Fire Research Laboratory
- Structures
- Building Materials
- Building Environment
- Fire Science and Engineering
- Fire Measurement and Research

Computer Systems Laboratory
- Information Systems Engineering
- Systems and Software Technology
- Computer Security
- Systems and Network Architecture
- Advanced Systems

Computing and Applied Mathematics Laboratory
- Applied and Computational Mathematics[2]
- Statistical Engineering[2]
- Scientific Computing Environments[2]
- Computer Services[2]
- Computer Systems and Communications[2]
- Information Systems

---

[1] At Boulder, CO 80303.
[2] Some elements at Boulder, CO 80303.

Semiconductor Measurement Technology:

User's Manual for the Program MONSEL-1: Monte Carlo Simulation of SEM Signals for Linewidth Metrology

Jeremiah R. Lowney

Semiconductor Electronics Division
Electronics and Electrical Engineering Laboratory
National Institute of Standards and Technology
Gaithersburg, MD 20899-0001

and

Egon Marx

Precision Engineering Division
Manufacturing Engineering Laboratory
National Institute of Standards and Technology
Gaithersburg, MD 20899-0001

August 1994

U.S. DEPARTMENT OF COMMERCE, Ronald H. Brown, Secretary
TECHNOLOGY ADMINISTRATION, Mary L. Good, Under Secretary for Technology
NATIONAL INSTITUTE OF STANDARDS AND TECHNOLOGY, Arati Prabhakar, Director

National Institute of Standards and Technology Special Publication 400–95
Natl. Inst. Stand. Technol. Spec. Publ. 400–95, 43 pages (Aug. 1994)
CODEN: NSPUE2

U.S. GOVERNMENT PRINTING OFFICE
WASHINGTON: 1994

For sale by the Superintendent of Documents, U.S. Government Printing Office, Washington, DC 20402–9325

Semiconductor Measurement Technology:
User's Manual for the Program MONSEL-I:
Monte Carlo Simulation of SEM Signals
for Linewidth Metrology

TABLE OF CONTENTS

LIST OF FIGURES

Semiconductor Measurement Technology:
User's Manual for the Program MONSEL-I:
Monte Carlo Simulation
of SEM Signals for Linewidth Metrology

Jeremiah R. Lowney
Semiconductor Electronics Division
Electronics and Electrical Engineering Laboratory
National Institute of Standards and Technology
Gaithersburg, MD 20899

and

Egon Marx
Precision Engineering Division
Manufacturing Engineering Laboratory
National Institute of Standards and Technology
Gaithersburg, MD 20899

ABSTRACT

This user's manual is a guide to the FORTRAN code MONSEL-I which is a Monte Carlo simulation of the transmitted and backscattered electron signals in a scanning electron microscope (SEM) associated with a line specimen with a trapezoidal cross section. The line is deposited on a multi-layer substrate. The primary purpose of the code is to determine the actual linewidth from measured SEM signals. However, it can be used for many other purposes such as transmission electron microscopy. Future extensions to model secondary electron signals and multiple lines are planned.

Key words: backscattered electrons; electron transmission; linewidth; Monte Carlo simulation; scanning electron microscope; X-ray lithography.

INTRODUCTION

The FORTRAN code MONSEL-I was written to simulate the linewidth measurements carried out on a metal line on top of a multilayer substrate placed in a scanning electron microscope (SEM) used in the transmission or backscattering mode. The simulation uses the Monte Carlo method, and the simulated specimens were x-ray lithographic masks.

The trajectories of the electrons in the beam are represented by straight lines between localized interaction sites, where the direction and the energy of the electron change. These changes are given by formulas that involve a random number which represents the probability of a particular change. Electrons can also dislodge other electrons (generated secondaries) at these interaction sites, and these electrons have separate trajectories. Electrons are counted when they leave the line or the substrate, or when their energies become too low while still inside the line or substrate. Electrons that have an energy of less than 50 eV when they leave the sample are called secondary electrons.

Future extensions of the code will model secondary signals more completely, as well as multiple lines on the same substrate. This present version, although aimed at a specific problem, should be useful for a number of simulation cases. Suggestions for further extensions are encouraged.

INSTALLATION

The code is essentially a stand-alone FORTRAN-77 code except for the incorporation of a random number generator (see below). The source code (approximately 73 kB) and sample input and output data files are available in ASCII format on disk or by using electronic mail over the Internet. The code is straightforward to run once the source has been compiled and linked by the user. The sample input and output data files are included so that the user can check the programs for proper operation as well as to become acquainted with the setup and use of the codes.

The code can run on nearly any machine, but hardware and software to speed up the execution should be considered by the user. A typical calculation of 80 points across a line with 20,000 electrons per point requires about 8000 s on a Cray Y-MP.[1] Such a calculation can take 20 h on a workstation. The memory requirements are relatively small. The executable is only 1.12 MB in length, which should fit on most machines. Although the code should perform correctly on all input data sets, there is no assurance that the code will perform equally well on all such data sets. Therefore, the authors and NIST assume no liability for possible losses resulting from the use of this code.

RANDOM-NUMBER GENERATOR

The heart of any Monte Carlo code is the random-number generator. The present code runs on a Cray Y-MP and several workstations at NIST. The code must be modified to call the random-number

---

[1] Certain commercial equipment is identified in this report in order to describe the experimental procedure adequately. Such identification does not imply recommendation or endorsement by NIST, nor does it imply that the equipment identified is necessarily the best available for the purpose.

generator (numbers are between 0 and 1) present on the user's computer. The Cray version, which is being made available, calls RANSET(0) in subroutine RNDSET to initialize the random-number generator and user function RANF() in function RNDFUN() to obtain the random numbers. The Cray names will have to be changed to agree with the user's supplied functions. Subroutine RNDSET and function RNDFUN() contain the Cray routines and must be edited before compilation. These subprograms should be "inlined" for efficient execution.

GENERAL SPECIMEN SHAPE

The shape of the specimen is shown in figure 1, which displays a cross section perpendicular to the translationally invariant line. The substrate can have up to three different layers, and all layers and the line can have four constituents. The layers in the present code are chromium, polyimide, and silicon; they can be changed by editing MONSEL.DAT, which uses free-format data lines under headers. The line is trapezoidal in cross section with a jog symmetrically located along both edges. The jog can be at any height along the edge and can have any width. The line is presently gold although it can be any material by editing MONSEL.DAT. The trapezoidal cross section can also model an undercut if the angle is negative, but then the jog height and width must be set to zero.

STRUCTURE OF THE PROGRAM

A call to INPT from MAIN inputs the data files MONSEL.IN and MONSEL.DAT along with the physical constants. In the MAIN program, the electrons are subdivided into groups of 200 electrons each to take advantage of vector processing. The variable *NI* in the PARAMETER statements throughout the code would have to be changed to change the value from 200, which is *NI*/5 where *NI* is presently 1001. The main loop starts with a computation for the incident electrons and then processes the electrons until all electrons are either backscattered, transmitted, or have been dropped if their energy is below the cutoff energy. The incident electrons are in a beam of given energy, diameter, and position, perpendicular to the plane of the sample.

The incident direction is normal to the substrate. A call to SBEAM distributes the electrons according to a Gaussian distribution determined by the beam diameter. There is a test to see whether the electrons hit the line or the substrate. The initial coordinates of each electron are computed in SBEAM. The initial elastic mean free path is computed in MFP.

In the repeating part of the main loop:

- a call to XSEC determines the scattering angle and the step to the new position,
- a call to GEOM determines the new direction cosines from the old ones and the scattering angle,
- a call to BOUND determines whether any boundaries have been crossed, dropping those electrons that have been transmitted or backscattered, and those for which the energy at a boundary goes below the cutoff energy,
- a call to ELOSS calculates the energy loss of the electron when it reaches its new position,
- a call to SCND determines whether any secondary electrons have been produced by ionization of valence electrons, and

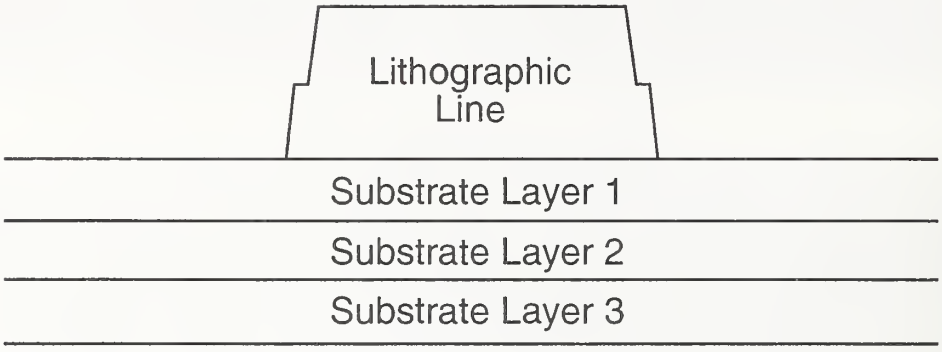

Figure 1. Diagram of general specimen shape.

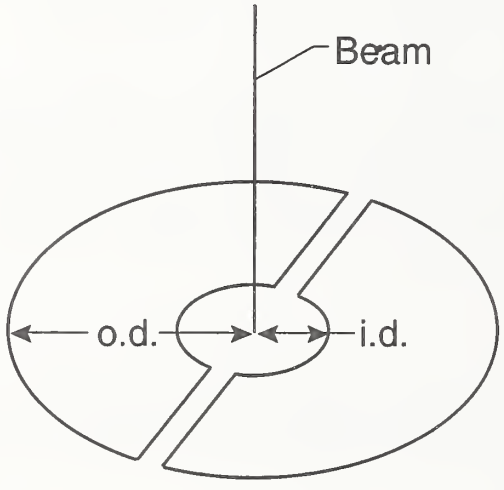

Figure 2. Diagram of backscattered-electron detector.

- the arrays are rearranged to eliminate the dropped electrons.

In the subroutine BOUND, the sequence of computations is:

for those electrons that started out in the substrate:

- transmitted electrons, i.e., those that end up under the substrate, are dropped after information on their energy and location is recorded, if desired, as well as whether they hit a detector with a defined aperture, separation distance, and low energy cutoff.
- the remainder may leave one of the layers of the substrate,
- those that leave the substrate and miss the line are backscattered and dropped,
- for those that hit the line, the energy at the interface is calculated by a call to SELOSS; if the energy is below the cutoff they are dropped, and the remaining electrons are left at the intersection with the line;

for the remaining electrons that started out in the line:

- those that end up above the line are backscattered and are dropped,
- those that remain within the height range of the line are checked to see whether they cross the sides,
- those that remain in the line are left alone,
- those that cross the side and are moving upwards are either backscattered or reenter the line,
- those that cross the side and are moving down end up in the substrate or back in the line,
- for those that end up in the substrate or line the intersection coordinates are determined, the energy at the interface is calculated by a call to SELOSS; if the energy is below the cutoff they are dropped, and the remainder are set at the interface.
- Note that backscattered electrons with energy below 50 eV are called secondaries, and that generated secondary electrons, which may have any energy, are deleted if they are generated by an electron that crosses a boundary.

The output files are: MONOUT, which gives a detailed account of each computed position across the line; MONSEL.OUT, which gives the backscattering coefficient, secondary yield (not fully functioning yet), total transmitted, and detected transmitted signals as a function of position across the line; MONBD.OUT, which gives the backscattered signal detected by a split-donut detector (see fig. 2); and MONSEL.TR, which gives the x,y positions of all the electrons for trajectory plotting. A practical number of electrons for trajectory plotting is 20. Examples of all the input and output files are given in the Appendix I.

COMPUTATION OF CROSS SECTIONS

Both the elastic cross section and the cross section for the generation of secondary electrons are considered.

The elastic cross section σ_e [cm^2] is given by Browning's fit to the Mott cross section [1]:

$$\sigma_e = 3\times10^{-18}Z^{1.7}/(E+0.005Z^{1.7}\sqrt{E}+0.0007Z^2/\sqrt{E}) , \quad (1)$$

where Z is atomic number and E is energy in kiloelectron volts.

The corresponding mean free path is

$$\lambda_e = \frac{A}{N_A\rho\sigma_e} , \quad (2)$$

where N_A is Avogadro's number, A is atomic weight, and ρ is density.

Browning obtained the differential elastic cross sections by assuming that they result from a sum of screened Rutherford and isotropic scattering. One reason for choosing these two forms is that they both have simple, analytic expressions for the differential cross sections, which can be readily evaluated by the code at each scattering event. Monte Carlo codes generally have long running times to achieve accuracy, and it is imperative that the numerical evaluations be done as quickly as possible. The use of look-up tables (even after spline fitting) for the true differential Mott cross sections would be very time-consuming. Browning adjusted the ratio r of the screened Rutherford to isotropic scattering so that he obtained the same ratio of total forward-to-backward scattering cross section as from the true Mott cross sections:

$$r = 300\frac{E}{Z} + \frac{Z^3}{3\times10^5 E} . \quad (3)$$

The screening parameter α in the Rutherford scattering was taken to $7 \times 10^{-3}/E$ for all Z.

Secondary electrons may be generated when the energy is above a cutoff energy, W_c, which may be higher than the minimum energy for the scattering of electrons. Only ionization of valence electrons has been considered so far. Other mechanisms will be included in later versions. For a fast secondary electron of energy W obtained by ionizing a valence electron by a primary electron of energy E, Møller's differential cross section is given by [2]:

$$d\sigma_{se}/dW = \frac{\pi e^4}{(4\pi\varepsilon_o)^2 E}\left[\frac{1}{W^2} + \frac{1}{(E-W)^2} - \frac{1}{W(E-W)}\right] , \quad (4)$$

which can be integrated starting from a minimum value $\epsilon_m = W_c/E$ to give:

$$\sigma_{se} = \frac{\pi e^4}{(4\pi\varepsilon_o)^2 E^2}\left[\frac{1}{\varepsilon_m} - \frac{1}{(1-\varepsilon_m)} - \ln\left[\frac{1-\varepsilon_m}{\varepsilon_m}\right]\right] . \quad (5)$$

The probability for obtaining a value of the reduced energy of the secondary electron between ϵ_m and $\epsilon = W/E$ is the integral

$$P(\varepsilon) = \frac{1}{\sigma_{se}} \int_{\varepsilon_m}^{\varepsilon} \frac{d\sigma_{se}}{d\varepsilon} d\varepsilon \tag{6}$$

which is a number that goes from 0 to 1 as ε goes from ϵ_m to 0.5. Given a random number, R, between 0 and 1, for this probability, the reduced energy ε that corresponds to this number can be determined.

The partial cross section up to an arbitrary energy ε is obtained as well, and both it and eq (5) involve a logarithmic term. This term presents difficulties when solving for the secondary-electron energies in terms of random numbers generated by the Monte Carlo routine. Thus, a rational polynomial function has been used, $(A + B\varepsilon + C\epsilon^2 + D\epsilon^3)/(1 + E\varepsilon + F\epsilon^2)$, to fit the following function $f(\varepsilon)$ to better than 1% throughout:

$$f(\varepsilon) = 1 - \varepsilon/(1-\varepsilon) - \varepsilon \ln [(1-\varepsilon)/\varepsilon], \; 0 \le \varepsilon \le 0.5 \; , \tag{7}$$

where $A = 0.988798$, $B = 0.220312$, $C = -9.16690$, $D = 9.53217$, $E = 4.95919$, and $F = -10.5818$. The solutions for the cross sections, thus, only involve the solution of a cubic equation, which saves considerable computer time instead of dealing with the logarithmic term.

In the subroutine SCND, the computations for the secondary electrons are carried out by assuming that the new electron is the one with the lower energy, which has to be above the cutoff. The energy of this electron is computed with the help of a random number generator, and so are the direction and the starting location. The scattering angle and step of the primary electron are computed with the formulas for elastic scattering for the next step.

The cross section for secondaries is, multiplying by the number of valence electrons Z_v [3] in an atom,

$$\sigma_{se}^{T} = 6.51\times10^{-20} Z_v/E^2 \left[\frac{1}{\varepsilon_m} - \frac{1}{(1-\varepsilon_m)} - \ln \left[\frac{1-\varepsilon_m}{\varepsilon_m} \right] \right] . \tag{8}$$

The mean free path for the production of secondary electrons is

$$\lambda_{se} = \frac{A}{N_A \rho \sigma_{se}^{T}} . \tag{9}$$

The probabilities of generating a secondary electron or undergoing elastic scattering are proportional to the corresponding cross sections. A random number r between 0 and 1 is generated, and a secondary electron occurs if

$$r < \sigma_{se}/(\sigma_e + \sigma_{se}) = \lambda_e/(\lambda_e + \lambda_{se}) . \tag{10}$$

The total cross section is

$$\sigma_{tot} = \sigma_e + \sigma_{se} \tag{11}$$

and the total mean free path is

$$\lambda_{tot} = \lambda_e\lambda_{se}/(\lambda_e + \lambda_{se}) \ . \tag{12}$$

The step is obtained from the corresponding mean free path λ by multiplying λ by another random number,

$$d = - \lambda\log(RND) \ , \tag{13}$$

where *RND* is a uniformly distributed random number between 0.000001 and 0.999999. The scattering angle is negligible in the event of the generation of a secondary electron, and for elastic scattering the cosine of the scattering angle for screened Rutherford scattering is given by

$$\cos(\theta) = 1 - \frac{2\alpha RND}{1 + \alpha - RND} \ , \tag{14}$$

where *RND* is another random number uniformly distributed between 0 and 1. For isotropic scattering the scattering angle is uniformly distributed.

If the computed step takes the electron from one medium to another, as determined in the subroutine BOUND, it is assumed that electron reaches the boundary without suffering a scattering event, but the energy is decreased by using the modified Bethe formula [4]. Then the possibility of another scattering event in the new medium is considered.

COMPUTATION OF ENERGY LOSS

The energy loss in eV/nm is obtained from Bethe's formula modified by Joy and Luo [4],

$$dE/dS = \frac{-7850\rho Z}{AE} \ln[1.166(E + 0.85J)/J] \ , \tag{15}$$

where J is the mean ionization potential in electron volts,

$$J = 9.76Z + 58.5/Z^{0.19}, \ Z \geq 13; \quad J = 11.5Z, \ Z \leq 12 \tag{16}$$

and S, ρ, and A are path length (nm), density (g cm^{-3}), and atomic weight (g), respectively. Equation (15) is valid for energies E above 8×10^{-3} J in electron volts.

COMPUTATION OF NEW DIRECTION COSINES

The new direction cosines A', B', and C', are defined in terms of the polar angle Θ and azimuthal

angle Φ in a coordinate system where the old direction cosines are (1,0,0), that is, where the electron is moving along the z-axis. There, Θ is the scattering angle and Φ is selected at random. To change from this coordinate system to the original one, a rotation about the x-axis by an angle θ is followed by a rotation about the new z-axis by an angle ϕ. The matrix of this product of rotations is:

$$\begin{bmatrix} \cos\phi & \sin\phi & 0 \\ -\sin\phi & \cos\phi & 0 \\ 0 & 0 & 1 \end{bmatrix} \begin{bmatrix} 1 & 0 & 0 \\ 0 & \cos\phi & \sin\theta \\ 0 & -\sin\theta & \cos\theta \end{bmatrix} = \begin{bmatrix} \cos\phi & \sin\phi\cos\theta & \sin\phi\sin\theta \\ -\sin\phi & \cos\phi\cos\theta & \cos\phi\sin\theta \\ 0 & -\sin\theta & \cos\theta \end{bmatrix} . \tag{17}$$

Then, the unit vector that has the original direction cosines as components can be obtained from the vector along the z-axis by this transformation,

$$\begin{bmatrix} A \\ B \\ C \end{bmatrix} = \begin{bmatrix} \cos\phi & \sin\phi\cos\theta & \sin\phi\sin\theta \\ -\sin\phi & \cos\phi\cos\theta & \cos\phi\sin\theta \\ 0 & -\sin\theta & \cos\theta \end{bmatrix} \begin{bmatrix} 0 \\ 0 \\ 1 \end{bmatrix} = \begin{bmatrix} \sin\phi\sin\theta \\ \cos\phi\sin\theta \\ \cos\theta \end{bmatrix} . \tag{18}$$

The new direction cosines in the original coordinate system can be obtained from those in the new coordinate system by a similar transformation, that is

$$\begin{bmatrix} A' \\ B' \\ C' \end{bmatrix} = \begin{bmatrix} \cos\phi & \sin\phi\cos\theta & \sin\phi\sin\theta \\ -\sin\phi & \cos\phi\cos\theta & \cos\phi\sin\theta \\ 0 & -\sin\theta & \cos\theta \end{bmatrix} \begin{bmatrix} \alpha \\ \beta \\ \gamma \end{bmatrix} \tag{19}$$

where the direction cosines in the new coordinate system are

$$\begin{bmatrix} \alpha \\ \beta \\ \gamma \end{bmatrix} = \begin{bmatrix} \sin\Theta\sin\Phi \\ \sin\Theta\cos\Phi \\ \cos\Theta \end{bmatrix} . \tag{20}$$

Thus:

$$\begin{bmatrix} A' \\ B' \\ C' \end{bmatrix} = \begin{bmatrix} \alpha\cos\phi + \sin\phi(\beta\cos\theta + \gamma\sin\theta) \\ -\alpha\sin\phi + \cos\phi(\beta\cos\theta + \gamma\sin\theta) \\ -\beta\sin\theta + \gamma\cos\theta \end{bmatrix} . \tag{21}$$

Given the direction cosines A, B, and C and the components of the new direction cosines in the rotated coordinate system, $\alpha(\Theta,\Phi)$, $\beta(\Theta,\Phi)$, and $\gamma(\Theta,\Phi)$, $\cos\theta$, $\sin\theta$, $\sin\phi$, and $\cos\phi$ are first determined from A, B, and C:

$$\cos\theta = C, \quad \sin\theta = (1 - C^2)^{1/2} , \quad \sin\phi = A/\sin\theta, \quad \cos\phi = B/\sin\theta . \tag{22}$$

Then, A', B', and C' are computed from α, β, and γ. When $\theta = 0$, we are already in a coordinate

system with the electron going along the z-axis, the angle ϕ is undetermined, and, for $\phi = 0$, the above equation reduces to

$$\begin{bmatrix} A' \\ B' \\ C' \end{bmatrix} = \begin{bmatrix} \alpha \\ \beta \\ \gamma \end{bmatrix} . \tag{23}$$

Similarly, when $\theta = \pi$, the angle ϕ is also undetermined, and

$$\begin{bmatrix} A' \\ B' \\ C' \end{bmatrix} = \begin{bmatrix} \alpha \\ -\beta \\ -\gamma \end{bmatrix} . \tag{24}$$

If $\pi - \Phi$ is needed instead of Φ, which is also a random angle, the sign of the y-component does not have to be changed, and:

$$\begin{bmatrix} A' \\ B' \\ C' \end{bmatrix} = \begin{bmatrix} \alpha \\ \beta \\ -\gamma \end{bmatrix} . \tag{25}$$

COMPUTATION OF INTERSECTION OF TRAJECTORIES WITH BOUNDARIES

This section corresponds to a trapezoidal line with no jog along the sides. The inclusion of the jog follows the same procedures outlined here, but with the further complications due to the additional ledge.

The base of the line is at $z = 0$, the top of the line is at $z = h$, centered about $x = 0$, and independent of y. The width of the top is $2w_1$ and the width of the base is $2w_2$. The thickness of the substrate is b, so that the bottom of the substrate corresponds to $z_b = -b$.

The direction cosines of the step are α, β, and γ, which are components of a unit vector $\hat{t}$. The final coordinates computed for that step are x_i, y_i, and z_i, forming the position vector $\vec{x}_i$. The step is s_i and the previous energy is E.

Assume first that the electron starts in the substrate. If the new position is below the substrate ($z \leq z_b$), the electron is transmitted and is no longer of interest. If there is a finite detector under the sample, the position of the electron at the detector coordinate is determined and a check is made as to whether it hits the detector itself.

If the electron crosses the top of the substrate, the coordinates of the point of intersection are found. The backward step is $s_b = z_i/\gamma$, and the coordinates of the intersection are $x_0 = x_i - s_b\alpha$, $y_0 = y_i - s_b\beta$, and $z_0 = 0$. The step inside the substrate is $s_0 = s_i - s_b$, which is used to compute the energy of the electron when it leaves the substrate.

The step to the top of the line, $s_t = h/\gamma$, and the x-coordinate at the top, $x_t = x_0 + s_t\alpha$, are calculated. Assume that the electron crosses into the vacuum at the right of the line, $x_0 > w_2$. If $x_t \geq w_1$, the electron does not hit the line. If the energy is greater than the threshold, 50 eV, the electron is considered to be backscattered; otherwise it is a secondary electron. If the electron hits the line, whether the remaining energy is greater than the cutoff energy is determined. If so, the intersection with the right side of the line is found. The equation of the trajectory of the electron is $\vec{x} = \vec{x}_0 + s\hat{t}$. The equation of the side of the line is $(x - w_2)/(w_1 - w_2) = z/h$. By letting $w_2 - w_1 = \Delta w$, the step is found to be:

$$s_1 = - h(x_0 - w_2)/(\alpha h + \gamma\Delta w) = - (x_0 - w_2)/(\alpha + \gamma\Delta w/h) \ . \tag{26}$$

Similarly, the intersection with the left side of the line corresponds to the step

$$s_2 = - h(x_0 + w_2)/(\alpha h - \gamma\Delta w) = - (x_0 + w_2)/(\alpha - \gamma\Delta w/h) \ . \tag{27}$$

If the electron leaves the substrate to the left of the line, $x_0 < - w_2$, the same computations are made with the appropriate changes. Otherwise, the electron crosses directly into the line, and the new step in the line is determined.

If the electron starts out in the line, it can end up above the line, $z_i \geq h$. First the intersection with the top, $\vec{x}_t = \vec{x}_i - s_b\hat{t}$, is determined from the back step $s_b = (z_i - h)/\gamma$. The electron exits through the right side if $x_t > w_1$. The intersection with the right side, $\vec{x}_s = \vec{x}_t - s_{s1}\hat{t}$ is determined as above, and

$$s_{s1} = h(x_t - w_1)/(\gamma\Delta w + \alpha h) \ . \tag{28}$$

Similarly, the intersection with the left side of the line corresponds to the step,

$$s_{s2} = - h(x_t + w_1)/(\gamma\Delta w - \alpha h) \ . \tag{29}$$

The remaining energy where it leaves the line is calculated. Figure 3 shows a diagram of these distances for an example trajectory.

If instead, the new electron position is in the substrate, the point where the electron enters the substrate is determined, given by $\vec{x}_0 = \vec{x}_i - s_b\hat{t}$, where $s_b = z_i/\gamma$ ($z_i < 0$, $\gamma < 0$). If it leaves through the side, the exit point $\vec{x}_s = \vec{x}_0 - s_s\hat{t}$ is determined. If it exits through the right side,

$$s_{s1} = h(x_0 - w_2)/(\alpha h + \gamma\Delta w) \ . \tag{30}$$

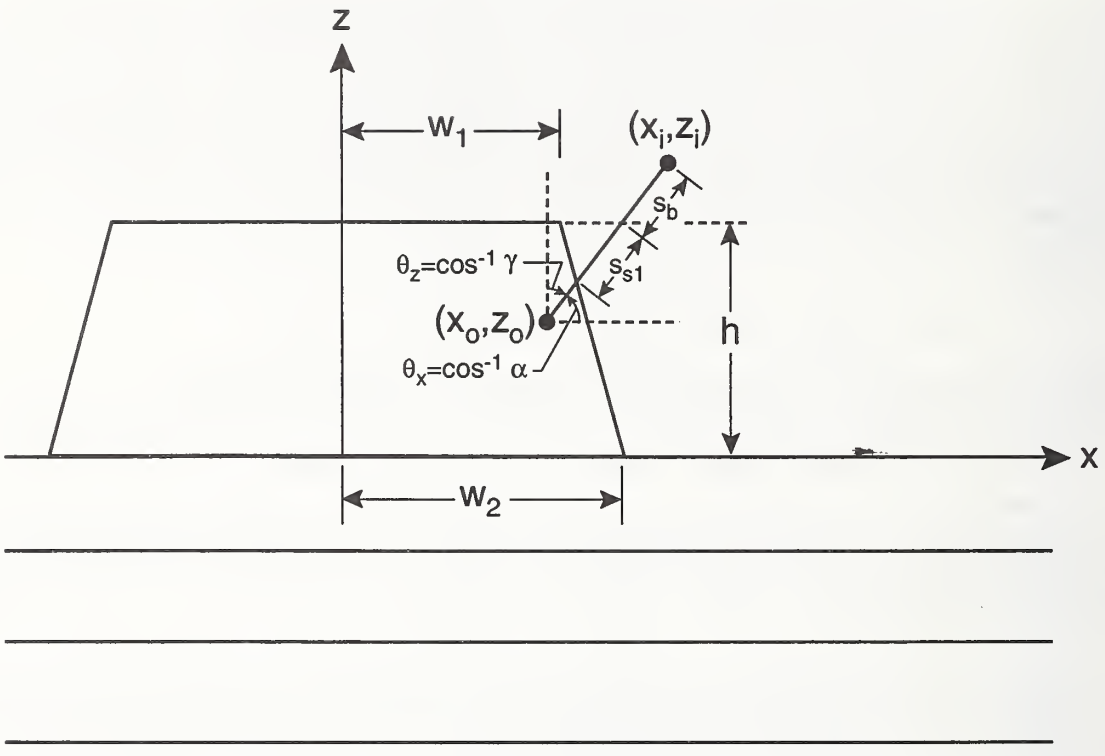

Figure 3. Diagram of an example of an intersection of an electron trajectory with the edge of a trapezoidal line.

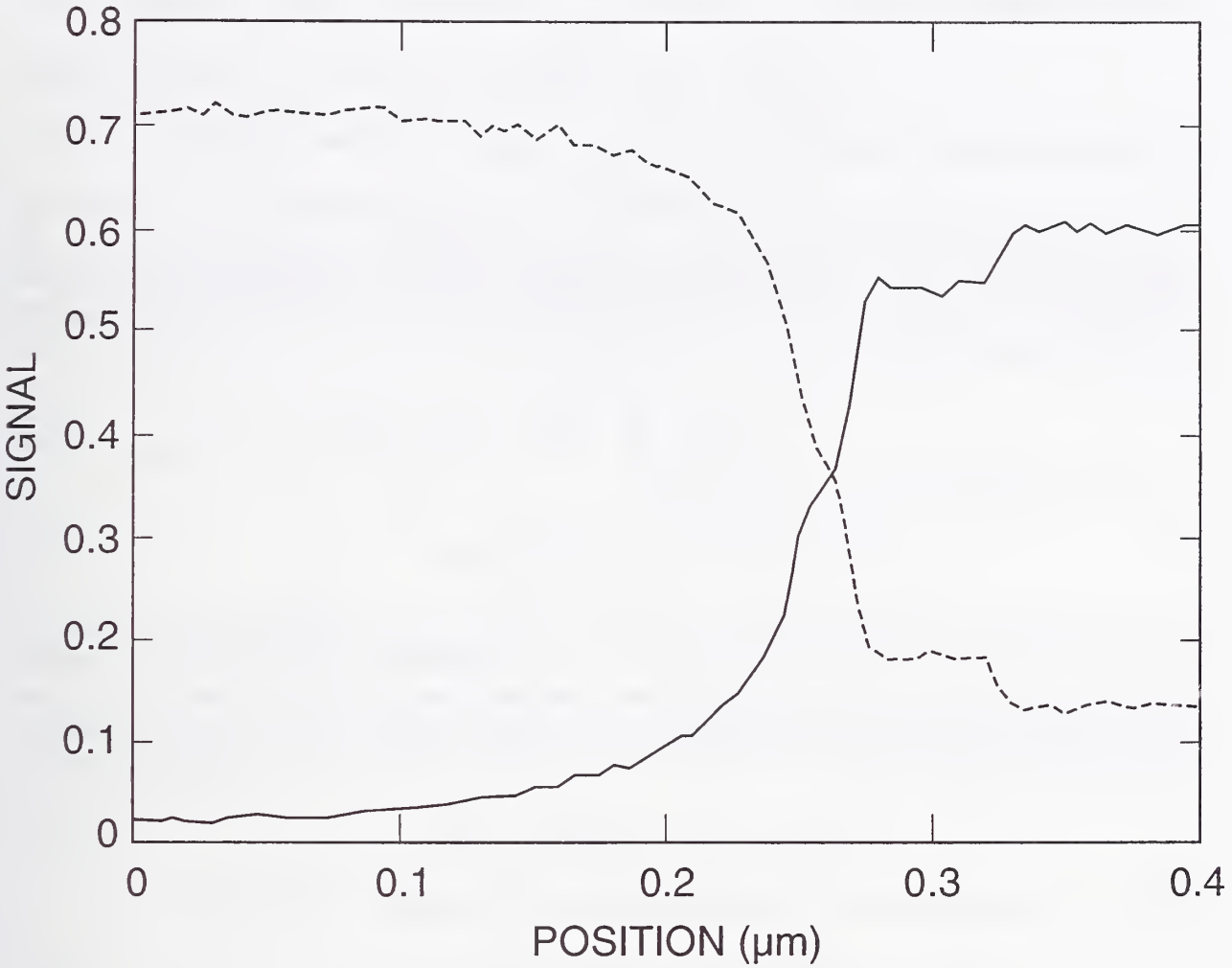

Figure 4. Calculated transmission (solid) and backscattering coefficient (dashed) for half of a 0.5-μm line with a 2-deg wall slope and a 50-nm jog 25 nm above the bottom.

If it exits through the left side,

$$s_{s2} = h(x_0 + w_2)/(\alpha h - \gamma \Delta w) \ . \tag{31}$$

The remaining energy is determined as well as the new step in the substrate and new final position.

The remaining case corresponds to an electron with a z-component such that $0 < z_i < h$. To find out whether it left the line, the distance from the point to the sides of the line, projected on the $y = 0$ plane is determined. If one of these distances is negative, the electron has left the line. A normal to the right side of the line is $\vec{N} = h\vec{\imath} + \Delta w\vec{k}$, and the scalar product with the vector from the new position to the base of the line, $(w_2 - x_i)\vec{\imath} - z_i\vec{k}$, gives

$$g_1 = h(w_2 - x_i) - z_i \Delta w \ . \tag{32}$$

The corresponding quantity for the other side is

$$g_2 = h(w_2 + x_i) - z_i \Delta w \ . \tag{33}$$

If both are positive, the electron remains in the line. If one of these is negative, the intersection of the trajectory of the electron with the corresponding side is computed and the step in the line and the remaining energy are determined. If the electron is directed down, the location where the electron hits the substrate is computed, as well as the new step. The intersection with the right side of the line is now given by the back step

$$s_1 = [z_i \Delta w + h(x_i - w_2)]/(\gamma \Delta w + \alpha h) \ . \tag{34}$$

Similarly, the intersection with the left side of the line corresponds to the back step

$$s_2 = [z_i \Delta w - h(x_i + w_2)]/(\gamma \Delta w - \alpha h) \ . \tag{35}$$

Figure 4 shows an example of the transmitted (solid) and backscattered (dashed) electron signals for half of a 0.5-μm gold line, 0.7-μm thick, with a 2-deg wall slope and a 50-nm jog 25-nm above the bottom of the line. The substrate is 2.5 μm of silicon with a 5-nm layer of chromium on top. The beam energy is 30 keV with a 10-nm diameter and 20,000 trajectories. The remaining parameters are given by the last four lines of data of MONSEL.IN in Appendix I.

MATERIAL CONSTANTS

The constants for silicon are $\rho = 2.328$ g/cm^3, $Z = 14$, and $A = 28.09$.
For gold, they are $\rho = 19.32$ g/cm^3, $Z = 79$, and $A = 196.97$.
For chromium, they are $\rho = 6.52$ g/cm^3, $Z = 24$, and $A = 52.01$.
For polyimide, there are four components: carbon, hydrogen, nitrogen, and oxygen. $\rho = 1.42$ g/cm^3, Z(C) = 6, Z(H) = 1, Z(N) = 7, and Z(O) = 8. The corresponding values of A are: 12.011, 1.008, 14.008, and 16.

Since the material in one of the layers has several components, the way the cross sections and the

mean free paths are computed must be changed. Several cross sections σ_i exist for each component. The mean free path that corresponds to σ_i is

$$\lambda_i = \frac{A_i}{N_A \rho c_i \sigma_i} \tag{36}$$

where c_i is the weight fraction for the i^{th} component. For polyimide the weight fractions of carbon, hydrogen, nitrogen, and oxygen are 0.6911, 0.0264, 0.0733, and 0.2092, respectively. The total mean free path is given by

$$1/\lambda = \sum 1/\lambda_i \ . \tag{37}$$

For the energy loss, the modified Bethe formula changes to

$$\frac{dE}{ds} = -78500 \frac{\rho}{E} \Sigma \frac{c_i Z_i}{A_i} \log \left[\frac{1.166(E + 0.85 J_i)}{J_i} \right] , \tag{38}$$

where J_i is the mean ionization potential.

A similar approach has to be followed for secondary electrons. There are different cross sections depending on which atom is involved. The mean free path for the production of secondary electrons for each constituent is

$$\lambda_{ise} = \frac{A_i}{N_A \rho c_i \sigma_{ise}} , \tag{39}$$

and the total mean free path for the production of secondary electrons is obtained from

$$1/\lambda_{se} = \Sigma 1/\lambda_{ise} \ . \tag{40}$$

SUMMARY

This manual describes the operation of the FORTRAN code MONSEL-I, which computes the electron transmission and backscattering signals from a trapezoidal line on a multi-layer substrate placed in a scanning electron microscope. The theoretical techniques involved are discussed in this manual as well as in Appendix II. Examples of input and output data appear in Appendix I. This code has been designed primarily for the measurement of linewidths on x-ray lithographic masks, but can have wide applications to simulate the interaction of electron beams and specimens.

REFERENCES

[1] R. Browning, T. Eimori, E. P. Traut, B. Chui, and R. F. W. Pease, An elastic cross section model for use with Monte Carlo simulations of low energy electron scattering from high atomic number targets, J. Vac. Sci. Technol. B Vol. 9 (6), pp. 3578-3581 (Nov. 1991).

[2] L. Reimer, Scanning Electron Microscopy (Springer-Verlag, New York, 1985), pp. 75-77.

[3] M. Cardona and L. Ley, Photoemission in Solids I, Topics in Applied Physics 26 (Springer-Verlag, New York, 1978), pp. 265-274.

[4] D. C. Joy and S. Luo, An Empirical Stopping Power Relationship for Low-Energy Electrons, Scanning Vol. 11 (4), pp. 176-180 (1989).

APPENDIX I

INPUT AND OUTPUT DATA FILES

The following pages give sample input and output data. These files must be in the same directory as the running code. The input file is MONSEL.IN. The entries are on data lines in free format preceded by header lines. This is true for all input files. The units are shown in each header. The first data line refers to the trajectory plot. If a trajectory plot is desired, the flag is true and the top, bottom, and total width of the frame are given. The second data line specifies the height and the width of the top of the line being measured, and the angle refers to the slope of the trapezoidal edge (see fig. 1). The third data line specifies the height and width of the jog along the edges, and the fourth data line specifies the thickness of the three layers that form the substrate. The fifth data line specifies the beam diameter, its initial and final positions, and the spacing between points. The sixth data line specifies the number of trajectories per point and the incident beam energy. The seventh data line specifies the distance between the sample and the transmission-signal detector, which is mounted concentric to the center of the line, the detector aperture (diameter), and cutoff energy. The eighth data line specifies the distance between the sample and the backscattered - electron detector (e.g., micro-channel plate or semiconductor diode detector), its inner and outer diameters (see fig. 2), its collection efficiency, and cutoff energy. The ninth data line specifies the lowest energy an electron can have before being dropped, and the tenth data line specifies the lowest energy a generated secondary electron may have. Setting both to 50 V eliminates collected secondaries.

MONSEL.DAT supplies the atomic numbers (*Z*), atomic weights (*A*), and densities (*RHO*) in grams per cubic centimeter of the line and three substrate layers. The number of component elements of each layer (*NCE*), weight fraction (*WF*), and the number of valence electrons (*NVE*), for each component are also given. Any element may be entered, and the entries are in free format under the headers.

MONOUT furnishes a detailed summary of the signals at each point. The first set of lines recapitulates the input data, the next set summarizes the output. The letters *L* and *R* in parentheses refer to the left half and right half of the backscattered-electron detector. The letters *S* and *D* in parentheses refer to the sum of both halves and the difference obtained by subtracting the right from the left half, respectively. The energy distributions (between *E1* and *E2*) of the electrons are given in the following tables. The first is for total backscattered, total transmitted, and detected transmitted electron signals. The second corresponds to the detected backscattered electron signal with the same notation as above.

MONSEL.OUT gives the total backscattered, secondary, total transmitted, and detected transmitted electron signals as a function of position. It is very useful if there is more than one point. The initial lines recapitulate the input data.

MONBD.OUT is like MONSEL.OUT except that it refers to detected backscattered-electron signals. The entries are: position, backscattered electron signal in the left half of the detector, same in the right half, their sum, and the right half subtracted from the left.

MONSEL.TR provides the initial and final positions of each electron step for trajectory plotting. All entries are in centimeters. The initial lines in the file are:

line 1) the half-width, top, and bottom of the plot frame;
line 2) the height, top half-width, and bottom half-width of the line;
line 3) the bottom of the first, second, and third layers;
line 4) the height, half-width of inner separation, and width of the jogs.

The remaining lines are initial x,z positions of the electron followed by the corresponding final position along each trajectory. The first few lines are shown for the same case as in the prior files but for only one electron.

```
traj. plot: flag  frame:     top(um)    bottom(um)    width(um)
            F                1.0        -3.0          4.0
line: height(um)    width(um)    angle (deg.)
      0.7           0.5          2.0
jog:  height(um)      width(nm)
      0.35            20.0
substrate: layer 1(um)    layer 2(um)    layer 3(um)
           5.0e-1         0.5            0.5
beam: diam.(nm)  init. pos.(um)  fin. pos.(um)  spacing of pts.(nm)
      10.0       0.0             0.0            5.0
no. inc. el.   beam energy(keV)
20000          30.0
trans. det.: dist.(mm)  aperture(mm)  cutoff en.(keV)
             5.0        12.5          16.0
bcksc. det.: dist.(mm)   id(mm)   od(mm)    eff.   cutoff en.(keV)
             5.0         2.5      12.5      1.0    16.0
minimum electron energy considered in calculation (eV)
50.0
minimum electron energy of generated secondary electron (eV)
50.0
```

MONSEL.DAT

Z	A(g)	RHO(g/cm3)	NCE	WF	NVE
LINE: ELEMENT IS GOLD					
		19.32	1		
79.	196.97			1.	11
FIRST LAYER: ELEMENT IS CHROMIUM					
		6.52	1		
24.	52.01			1.	6
SECOND LAYER: COMPOUND IS POLYIMIDE (C, H, N, O)					
		1.42	4		
6.	12.011			0.6911	4
1.	1.008			0.0264	1
7.	14.008			0.0733	3
8.	16.			0.2092	4
THIRD LAYER: ELEMENT IS SILICON					
		2.328	1		
14.	28.09			1.	4

```
BEGIN OUTPUT
HEIGHT OF LINE IS  7.000E-01 um
HALF-WIDTH OF TOP OF LINE IS  2.500E-01 um
HALF-WIDTH OF BOTTOM OF LINE IS  2.944E-01 um
HEIGHT OF JOG IS  3.500E-01 um
WIDTH OF JOG IS  2.000E+01 nm
THICKNESS OF THE FIRST LAYER IS  5.000E-01 um
THICKNESS OF THE SECOND LAYER IS  5.000E-01 um
THICKNESS OF THE THIRD LAYER IS  5.000E-01 um
BEAM DIAMETER IS  1.000E+01 nm
BEAM STARTS AT X= 0.000E+00, ENDS AT X= 0.000E+00 um
NUMBER OF POINTS:   1
NUMBER OF INCIDENT ELECTRONS:  20000
INCIDENT BEAM ENERGY:  3.000E+01 keV
DIST. TO DET. FOR TRANS. ELEC.:  5.000E+00 mm
APERTURE:  1.250E+01 mm
CUTOFF ENERGY OF DETECTOR:  1.600E+01 keV
DIST. TO DETECTOR FOR BACKSC. ELEC.:  5.000E+00 mm
IN. DIAM.:  2.500E+00 mm, OUT. DIAM.:  1.250E+01 mm
EFFICIENCY:  1.000E+00, CUTOFF EN.:  1.600E+01 keV
MINIMUM ELECTRON ENERGY CONSIDERED:  0.050 keV
MINIMUM GEN. SECONDARY ELECTRON ENERGY:  0.050 keV


LOCATION    1 WITH BEAM AT X= 0..000000E+00

NUMBER OF GEN. SECONDARY ELECTRONS IS   147448
NUMBER OF BACKSC. ELECTRONS IS  14500
NUMBER OF DET. BACKSC. EL. (L) IS   2590
NUMBER OF DET. BACKSC. EL. (R) IS   2536
SUM OF DET. BACKSC. EL. (S) IS   5126
DIFF. OF DET. B. EL., L-R, (D) IS     54
NUMBER OF SEC. ELECTRONS IS      0
TOTAL NUMBER OF TRANS. ELECTRONS IS   1672
NUMBER OF DET. TRANS. ELECTRONS IS    627
BACKSCATTERING COEFFICIENT =   7.250E-01
DETECTED BACKSC. COEFF. (L) =   1.295E-01
DETECTED BACKSC. COEFF. (R) =   1.268E-01
DETECTED BACKSC. COEFF. (S) =   2.563E-01
DETECTED BACKSC. COEFF. (D) =   2.700E-03
SECONDARY ELECTRON COEFFICIENT =   0.000E+00
TOTAL TRANSMITTED ELECTRON COEFF. =   8.360E-02
DET. TRANSMITTED ELECTRON COEFF. =   3.135E-02
```

ENERGY DISTRIBUTIONS

EN. BET. E1 AND E2 (keV)		NUMBER BACKSCAT	NUMBER TRANS	DET. TRANS.
0.00	1.00	63	4	0
1.00	2.00	30	7	0
2.00	3.00	28	5	0
3.00	4.00	43	16	0
4.00	5.00	45	10	0
5.00	6.00	65	20	0
6.00	7.00	70	24	0
7.00	8.00	74	29	0
8.00	9.00	96	48	0
9.00	10.00	126	56	0
10.00	11.00	130	60	0
11.00	12.00	151	73	0
12.00	13.00	158	101	0
13.00	14.00	213	109	0
14.00	15.00	252	139	0
15.00	16.00	257	157	0
16.00	17.00	316	168	121
17.00	18.00	409	170	125
18.00	19.00	438	173	128
19.00	20.00	501	118	94
20.00	21.00	636	107	90
21.00	22.00	726	53	45
22.00	23.00	920	22	21
23.00	24.00	1066	3	3
24.00	25.00	1254	0	0
25.00	26.00	1401	0	0
26.00	27.00	1434	0	0
27.00	28.00	1173	0	0
28.00	29.00	1122	0	0
29.00	30.00	1303	0	0

ENERGY DISTRIBUTIONS

EN. BET. E1 AND E2 (keV)		NUM. BCKSC(L)	NUM. BCKSC(R)	SUM	DIFF (L-R)
0.00	1.00	0	0	0	0
1.00	2.00	0	0	0	0
2.00	3.00	0	0	0	0
3.00	4.00	0	0	0	0
4.00	5.00	0	0	0	0
5.00	6.00	0	0	0	0
6.00	7.00	0	0	0	0
7.00	8.00	0	0	0	0
8.00	9.00	0	0	0	0
9.00	10.00	0	0	0	0
10.00	11.00	0	0	0	0
11.00	12.00	0	0	0	0
12.00	13.00	0	0	0	0
13.00	14.00	0	0	0	0
14.00	15.00	0	0	0	0
15.00	16.00	0	0	0	0
16.00	17.00	62	77	139	-15
17.00	18.00	93	83	176	10
18.00	19.00	83	86	169	-3
19.00	20.00	98	98	196	0
20.00	21.00	100	121	221	-21
21.00	22.00	119	129	248	-10
22.00	23.00	166	167	333	-1
23.00	24.00	182	197	379	-15
24.00	25.00	210	191	401	19
25.00	26.00	259	232	491	27
26.00	27.00	268	254	522	14
27.00	28.00	302	256	558	46
28.00	29.00	322	314	636	8
29.00	30.00	326	331	657	-5

```
HEIGHT OF LINE IS  7.000E-01 um
HALF-WIDTH OF TOP OF LINE IS  2.500E-01 um
HALF-WIDTH OF BOTTOM OF LINE IS  2.944E-01 um
HEIGHT OF JOG IS  3.500E-01 um
WIDTH OF JOG IS  2.000E+01 nm
THICKNESS OF THE FIRST LAYER IS  5.000E-01 um
THICKNESS OF THE SECOND LAYER IS  5.000E-01 um
THICKNESS OF THE THIRD LAYER IS  5.000E-01 um
BEAM DIAMETER IS  1.000E+01 nm
BEAM STARTS AT X= 0.000E+00, ENDS AT X= 0.000E+00 um
NUMBER OF POINTS:   1
NUMBER OF INCIDENT ELECTRONS:  20000
INCIDENT BEAM ENERGY:  3.000E+01 keV
DIST. TO DET. FOR TRANS. ELEC.:  5.000E+00 mm
APERTURE:  1.250E+01 mm
CUTOFF ENERGY OF DETECTOR:  1.600E+01 keV
DIST. TO DETECTOR FOR BACKSC. ELEC.:  5.000E+00 mm
IN. DIAM.:  2.500E+00 mm, OUT. DIAM.:  1.250E+01 mm
EFFICIENCY:  1.000E+00, CUTOFF EN.:  1.600E+01 keV
MINIMUM ELECTRON ENERGY CONSIDERED:  0.050 keV
MINIMUM GEN. SECONDARY ELECTRON ENERGY:  0.050 keV
```

X(um)	BS	SEC	TOT TR	DET TR
0.0000E+00	7.2500E-01	0.0000E+00	8.3600E-02	3.1350E-02

MONBD.OUT

HEIGHT OF LINE IS 7.000E-01 um
HALF-WIDTH OF TOP OF LINE IS 2.500E-01 um
HALF-WIDTH OF BOTTOM OF LINE IS 2.944E-01 um
HEIGHT OF JOG IS 3.500E-01 um
WIDTH OF JOG IS 2.000E+01 nm
THICKNESS OF THE FIRST LAYER IS 5.000E-01 um
THICKNESS OF THE SECOND LAYER IS 5.000E-01 um
THICKNESS OF THE THIRD LAYER IS 5.000E-01 um
BEAM DIAMETER IS 1.000E+01 nm
BEAM STARTS AT X= 0.000E+00, ENDS AT X= 0.000E+00 um
NUMBER OF POINTS: 1
NUMBER OF INCIDENT ELECTRONS: 20000
INCIDENT BEAM ENERGY: 3.000E+01 keV
DIST. TO DET. FOR TRANS. ELEC.: 5.000E+00 mm
APERTURE: 1.250E+01 mm
CUTOFF ENERGY OF DETECTOR: 1.600E+01 keV
DIST. TO DETECTOR FOR BACKSC. ELEC.: 5.000E+00 mm
IN. DIAM.: 2.500E+00 mm, OUT. DIAM.: 1.250E+01 mm
EFFICIENCY: 1.000E+00, CUTOFF EN.: 1.600E+01 keV
MINIMUM ELECTRON ENERGY CONSIDERED: 0.050 keV
MINIMUM GEN. SECONDARY ELECTRON ENERGY: 0.050 keV

X(um)	BSDL	BSDR	BSDSUM	BSDD(L-R)
0.0000E+00	1.2950E-01	1.2680E-01	2.5630E-01	2.7000E-03

```
 0.20000E-03   0.10000E-03  -0.30000E-03
 0.70000E-04   0.25000E-04   0.29444E-04
-0.50000E-04  -0.10000E-03  -0.15000E-03
 0.35000E-04   0.26222E-04   0.20000E-05
 0.25576E-06   0.10000E-03   0.25576E-06   0.69690E-04
 0.25576E-06   0.69690E-04   0.25838E-06   0.69595E-04
 0.25838E-06   0.69595E-04   0.26974E-06   0.69002E-04
 0.26974E-06   0.69002E-04   0.26981E-06   0.68997E-04
 0.26981E-06   0.68997E-04   0.26992E-06   0.68959E-04
 0.26992E-06   0.68959E-04   0.26931E-06   0.68891E-04
 0.26931E-06   0.68891E-04   0.26594E-06   0.68860E-04
 0.26594E-06   0.68860E-04   0.25178E-06   0.68729E-04
 0.25178E-06   0.68729E-04   0.22735E-06   0.68525E-04
 0.22735E-06   0.68525E-04   0.20027E-06   0.68320E-04
 0.20027E-06   0.68320E-04   0.14547E-06   0.67844E-04
 0.14547E-06   0.67844E-04   0.11883E-06   0.67495E-04
 0.11883E-06   0.67495E-04   0.11272E-06   0.67392E-04
 0.11272E-06   0.67392E-04   0.95091E-07   0.66844E-04
 0.95091E-07   0.66844E-04  -0.99394E-08   0.65794E-04
-0.99394E-08   0.65794E-04  -0.23519E-07   0.65667E-04
-0.23519E-07   0.65667E-04  -0.50896E-07   0.65528E-04
-0.50896E-07   0.65528E-04  -0.91678E-07   0.65331E-04
-0.91678E-07   0.65331E-04  -0.12471E-06   0.65166E-04
-0.12471E-06   0.65166E-04  -0.13976E-06   0.65094E-04
-0.13976E-06   0.65094E-04  -0.15320E-06   0.65040E-04
-0.15320E-06   0.65040E-04  -0.17525E-06   0.64948E-04
```

APPENDIX II

REPRINT OF A MONTE CARLO MODEL FOR SEM LINEWIDTH METROLOGY, BY J.R. LOWNEY, M.T. POSTEK, and A.E. VLADAR, PROCEEDINGS OF SPIE, Vol. 2196, pp. 85-96, 1994.

A Monte Carlo model for SEM linewidth metrology*

Jeremiah R. Lowney, Michael T. Postek, and Andras E. Vladar
National Institute of Standards and Technology
Gaithersburg, MD 20899

ABSTRACT

A scanning electron microscope (SEM) can be used to measure the dimensions of the microlithographic features of integrated circuits. However, without a good model of the electron-beam/specimen interaction, accurate edge location cannot be obtained. A Monte Carlo code has been developed to model the interaction of an electron beam with a line lithographically produced on a multi-layer substrate. The purpose of the code is to enable one to extract the edge position of a line from SEM measurements. It is based on prior codes developed at NIST, but with a new formulation for the atomic scattering cross sections and the inclusion of a method to simulate edge roughness or rounding. The code is currently able to model the transmitted and backscattered electrons, and the results from the code have been applied to the analysis of electron transmission through a gold line on a thin silicon substrate, such as used in an x-ray lithographic mask. By comparing the predictions of the code with measured data, it is possible to obtain edge positions to the order of ±10 nm, which is needed for the advanced lithography projected for the year 2000. The uncertainty of this measurement is limited by the sample geometry and surface roughness and not by the measurement process.

1. INTRODUCTION

As lithographically produced features on semiconductor wafers and masks become ever smaller (<0.1 μm), more demands are placed on the metrological tools used to measure their dimensions. The scanning electron microscope (SEM) offers the advantage of a very small electron wavelength and a beam diameter on the order of 1-10 nm depending upon instrument operating conditions. However, it has the disadvantage that the electron beam expands greatly within a solid due to atomic scattering, and thus, it is difficult to relate the collected signal electrons to their point of entry into the specimen. Theoretical modeling of the interaction between the electron beam and specimen is required to obtain meaningful dimensional information from the SEM signal images. To do so, accurate models for the elastic and inelastic scattering of electrons by the host atoms are needed. This work has used a Monte Carlo code that incorporates some of the most recent models for these effects. We have also carefully studied both experimentally and theoretically the signal behavior near line edges and extended our

---

previous work [1].

We have concentrated on transmitted and backscattered electron signals instead of the more common secondary-electron signal (i.e., from electrons with less than 50 eV) because the former can be more accurately modeled. Accurate first-principles theories for secondary electrons do not exist, and the usual treatment is to assume that the generation of secondaries is proportional to the energy loss of electrons as they traverse the sample. However, such a treatment is only semiquantitative because the energies and trajectories of individual secondary electrons are not known precisely. Secondary production affects the higher-energy transmitted and backscattered electrons only weakly, and reasonably accurate first-principles theories exist for elastic scattering and overall energy loss. We have applied these theories to calculate the transmitted and backscattered electron yields as a function of position across a lithographically produced trapezoidal line on a multi-layer substrate. From the results, we can obtain accurate and precise relationships between the measured SEM images and the dimensions of the line. We have simulated edge roughness or irregularities by placing a symmetric jog (i.e., a discontinuous change in the width of the trapezoid) along the trapezoidal line edges. The results show the sensitivity of the SEM signals to this perturbation. We have also studied the signal-to-noise ratio of the Monte Carlo calculations.

2. MONTE CARLO CODE

The code is designed to calculate the transmitted and backscattered electron distributions associated with a multi-layer specimen. As presently written, the specimen is composed of a trapezoidal gold line on top of a substrate consisting of silicon, polyimide, and chromium layers, representing an X-ray lithographic mask [1]. The specimen dimensions and the incident electron-beam energy, diameter, and positions are given as input. There is a provision for a jog of variable height and width to be placed symmetrically along the trapezoidal line edges to simulate the effects of edge roughness. There is also provision for a detector of variable aperture, distance, and cut-off energy to be used for measuring the electron transmission. A similar detector can be inserted for measuring the backscattered electron signal. The minimum energy of an electron in the specimen before it is removed from consideration can be entered as input, and in this work it is set to 50 eV so that outputted secondary electrons are not considered. There is provision for the generation of secondary electrons with energies above an inputted cut-off, equal in this work to 50 eV. However, only collisions with valence electrons are considered for secondary production because 1) the inclusion of core electrons requires specific empirical relations and their effects are relatively small, and 2) the treatment of plasmon-induced secondaries is very difficult and their effects, although large, are at low energies (<25 eV). The total number of trajectories used per beam position can be varied and needs to be around 20,000 for accurate results, which we use unless otherwise stated.

The code described here is an extension and modification of an earlier NIST Monte Carlo code [2]. The previous code used a modified screened-Rutherford model for elastic scattering, a simplification of the Møller formula [3] for inelastic scattering, and Rao Sahib and Wittry's correction [4] to Bethe's formula for energy loss [5]. The primary subroutines in both codes are: input and output, calculation of elastic mean free paths and scattering angles, calculation of energy loss due to inelastic scattering, calculation of secondary production, and determination of when an electron crosses the boundaries of either the trapezoidal line or multi-layer substrate. There is also a subroutine that distributes the input electron beam according to a Gaussian distribution.

The following discussion pertains to the new code. The elastic cross sections are now determined by fitted formulas obtained by Browning [6] to approximate the highly accurate Mott cross sections [7,8], which take into account the relativistic effects. First, Browning computed a relation for the total elastic cross section σ_T as a function of atomic number Z and electron energy E [keV], which includes the relativistic correction factor:

$$\sigma_T = 3\times10^{-18} Z^{1.7}/(E+0.005 Z^{1.7}\sqrt{E}+0.0007 Z^2/\sqrt{E})\ cm^2 \ . \tag{1}$$

Next he obtained the differential cross sections by assuming that they result from a sum of screened Rutherford and isotropic scattering. One reason for choosing these two forms is that they both have simple, analytic expressions for the differential cross sections, which can be readily evaluated by the code at each scattering event. Monte Carlo codes generally have long running times to achieve accuracy, and it is imperative that the numerical evaluations be done as quickly as possible. The use of look-up tables (even after spline fitting) for the true differential Mott cross sections would be very time consuming. Browning adjusted the ratio r of the screened Rutherford to isotropic scattering so that he obtained the same ratio of total forward-to-backward scattering cross section as from the true Mott cross sections:

$$r = 300\frac{E}{Z} + \frac{Z^3}{3X10^5 E} \ . \tag{2}$$

The main difference between his method and the actual use of Mott cross sections is that the oscillatory structure present in the differential Mott cross sections as a function of angle is replaced by a smooth average dependence. As long as the desired outputs result from partial integration over solid angle or from many scattering events, as is true in this work, the results are not very sensitive to this difference. However, if specific and accurate angular trajectories are desired, the actual Mott cross sections would be needed.

The energy loss per electron step is caused by inelastic scattering such as by the excitation of plasmons, inter- and intra-band transitions, and core excitations. We use Bethe's expression for the loss rate [5], modified by Joy and Luo [9] to be more accurate at lower energies E [eV]:

$$dE/dS = \frac{-7850\rho Z}{AE} \ln[1.166(E+0.85J)/J]\ eV/nm \ , \tag{3}$$

where

$$J = 9.76Z+58.5/Z^{0.19}\ eV,\ Z\geq13; \quad J = 11.5Z\ eV,\ Z\leq12 \tag{4}$$

and S, ρ, and A are path length [nm], density [g cm^{-3}], and atomic weight [g], respectively.

This is also the formula that Browning used to calculate backscatter coefficients in his work. Other treatments exist for modifying Bethe's formula so that it applies to low energy electrons, but our choice of Joy and Luo's method is adequate for our purposes because we never consider electrons

with energies below 50 eV, when the value of the logarithm could become zero or negative and thus be invalid.

The generation of secondary electrons has been dealt with only in an approximate way because the focus of the code is to simulate transmission and backscattering of electrons at energies above 50 eV, at which energies the contribution of secondary electrons is small. We have considered only the contribution of valence electrons to secondary production because they constitute an important contribution and can be modeled simply. Plasma contributions, which are at energies below 50 eV, need not be included; and core-electron contributions, which are usually smaller, require atomic-specific empirical relations as given by Gryzinski [3,10]. We have used the Møller formula [3] for the valence electrons:

$$d\sigma/dW = \frac{\pi e^4}{(4\pi\varepsilon_o)^2 E}\left[\frac{1}{W^2} + \frac{1}{(E-W)^2} - \frac{1}{W(E-W)}\right], \tag{5}$$

where $d\sigma/dW$ is the differential inelastic cross section for an energy loss between W and $W+dW$, E is the energy of the incident electron, and W is the energy of the secondary electron. We assume that E is much less than $m_o c^2$ = 511 keV so that the relativistic terms can be ignored. We define a reduced secondary energy $\varepsilon=W/E$ and integrate Eq. (5) from a minimum secondary energy ϵ_m to the maximum value of ε, 0.5, to obtain the total cross section:

$$\sigma = \frac{\pi e^4}{(4\pi\varepsilon_o)^2 E^2}\left[\frac{1}{\varepsilon_m} - \frac{1}{(1-\varepsilon_m)} - \ln\left[\frac{1-\varepsilon_m}{\varepsilon_m}\right]\right]. \tag{6}$$

The partial cross section up to an arbitrary energy ε is obtained as well, and both expressions involve a logarithmic term. This term presents difficulties when solving for the secondary-electron energies in terms of random numbers generated by the Monte Carlo routine. Thus, we have used a rational polynomial function, $(A + B\varepsilon + C\epsilon^2 + D\epsilon^3)/(1 + E\varepsilon + F\epsilon^2)$, to fit the following function $f(\varepsilon)$ to better than 1% throughout:

$$f(\varepsilon) = 1 - \varepsilon/(1-\varepsilon) - \varepsilon \ln[(1-\varepsilon)/\varepsilon],\ 0 \le \varepsilon \le 0.5, \tag{7}$$

where A = 0.988798, B = 0.220312, C = -9.16690, D = 9.53217, E = 4.95919, and F = -10.5818. The solutions for the cross sections, thus, only involve the solution of a cubic equation, which saves considerable computer time instead of dealing with the logarithmic term. Usually the logarithmic term has been neglected in such calculations, but this shows how it can be included efficiently.

Finally, there is a subroutine that determines when any electron crosses a boundary, either between layers or into empty space. The direction of the electron is needed upon crossing a boundary to know where it is heading. For example, electrons may exit and reenter the sample or they may be detected. The energy of a boundary-crossing electron must be calculated so that only the loss during the time the electron is in the starting material is counted. If secondaries are produced during a

boundary-crossing step, they are eliminated since it is less than a full mean-free path. If an electron has crossed a boundary into a new material or portion of the same material, the new step starts at the point of entry. The treatment of boundaries is more difficult than one might expect because of the need to model all possible scattering events. This prevents the modeling of generally rough surfaces. Instead, we have tried to model the effect of surface roughness or rounding by placing a jog along the trapezoidal line faces (symmetrically) that can vary in position and width. This one jog in principle accounts for a series of jagged edges.

3. RESULTS AND DISCUSSION

We show a general diagram of the specimens we can model in Fig. 1 and an SEM micrograph of an X-ray mask in figure 2. In a previous paper [1], we showed plots of the transmitted and backscattered electron signals from 0.7 μm-thick gold lines on 2.5 μm Si substrates separated by a 5 nm film of chromium. They were based on the version of the code we used at that time and were representative of X-ray masks. We present in Figs. 3-5 a revision of Fig. 10 of Ref [1] for the same specimens. These traces were obtained from 20,000 trajectories for an incident beam energy of 30 keV, beam diameter of 10 nm, and a transmission electron detector with a 16 keV cutoff energy and a 1.25 cm diameter, which was placed 5 mm below the sample. These parameter values are used throughout this paper unless otherwise stated. The curve in figure 3 was obtained from a nonlinear least-squares fit based on a rational polynomial function. The results of Figs. 3-5 are nearly the same as those of Ref. [1], which shows that the improvements to the code have not altered the numerical results significantly because the previous code had used internal adjustable factors to achieve good agreement with measured data. This new code uses only first-principle models, which are not adjusted. Again, we observe the short plateau-like feature near the middle of both the transmitted and backscattered signals as the beam traverses the trapezoidal line edge. Note that the width of the jog is zero. This feature is due to the "reflection-like" behavior of the electron beam when it impinges on a nearly vertical wall, and the plateau is due to the near independence of the signal on position along the edge. This plateau provides a method to identify the edge if the noise in the experimental signal is small enough.

Figures 6 and 7 show experimental data and theoretical simulation, respectively, of the detected electron transmission across a 0.5 μm gold line, on an X-ray mask with a field-emission SEM. The plots show transmission plotted downward so that the images correspond in shape to the elevated line. The wall angle for the calculated signal is 2 deg. Agreement between theory and experiment is very good, with the position of the plateau at nearly the same location in both figures.

The best fit between data and theory in our previous paper, as shown in Fig. 9 of Ref. [1], was obtained with an edge slope of 4 deg. However, SEM photographs indicated that the actual slope was only between 2 and 3 degs. We, thus, postulated that the extra "slope" was due to edge roughness. We have investigated the effect of edge roughness by including a small jog along the edge of the trapezoidal line. We show in Figs. 8 and 9 the changes in detected transmission and backscattering associated with placing a jog 0.25, 0.5, and 0.75 of the distance above the substrate. The width of the jog in each case was 20 nm, and the edge slope was 2 deg. The position of the jog in the signal that correlates with the jog along the edge moves somewhat with the jog placement as expected. It also more than accounts for the difference between the needed effective 4-deg edge slope and the measured 2-deg one. It is important to note that the plateau in the signals that occurs as the beam

traverses a clean sloped edge is similar to that created by a real jog along the edge. The first effect is the result of electrons emerging from the surface due to the small glancing angle. The second is due to an additional overhang of edge material. The presence of the jog obscures the plateau-like feature because the beam is not able to traverse the length of edge unobstructedly. The structure of the signal modification caused by the jog is interesting. Its shape is serpentine because of the angular beam trajectories that determine the signal. The transmission is relatively reduced and the backscattering coefficient relatively enhanced when the beam is centered over the jog.

We show in Fig. 10 the transmission and backscattering from a line with a 2-deg wall slope and a "foot," which is 25 nm high and 50 nm long. The feature is well represented in both signals. The noise associated with the Monte Carlo calculations is shown for various numbers of trajectories in Fig. 11. Transmission is plotted downward so that the figure conforms to the elevated line shape. A histogram of the standard deviation of the signal about its mean as a percentage of the maximum detected transmission is shown in Fig. 12. It is clear that about 10,000 trajectories are needed for a noise level of less than 1%. We have used 20,000 in the calculations shown here where the noise level is 0.5%. Above 50,000 there is hardly any visible noise left in Fig. 11, and a larger number than this seems unnecessary.

4. CONCLUSIONS

The NIST Monte Carlo code for SEM linewidth metrology has been improved and extended by incorporating the most recent models for electron scattering cross sections and adding a small jog along the sides of a trapezoidal line to model roughness. Results are shown for the transmission and backscattering of electrons from a gold line on a thin silicon substrate (with a chromium inter-layer). Experimental data have confirmed the existence of a predicted plateau in both the transmission and backscattering signals as the beam traverses the edge of the line. The addition of a jog along the edge was also investigated to study the effects of edge roughness and rounding. The X-ray lithography mask is a very good model system for the development of accurate SEM standards because it provides a measurement of both transmitted and backscattered electrons for comparison with predictions of theoretical models.

5. REFERENCES

1) M. T. Postek, J. R. Lowney, A. E. Vladar, W. J. Keery, E. Marx, and R. D. Larrabee, "X-ray Lithographic Mask Metrology: Use of Transmitted Electrons in an SEM for Linewidth Measurement," J. Res. Natl. Inst. Stand. Technol., Vol. 98(4), pp 415-445, July 1993.

2) R. L. Myklebust, D. E. Newbury, and H. Yakowitz, "NBS Monte Carlo Electron Trajectory Calculation Program," NBS Special Publication 460, Edited by K. Heinrich, D. Newbury, and H. Yakowitz, pp. 105-125, U. S. Govt. Printing Office, Washington, DC, Dec. 1976.

3) L. Reimer, Scanning Electron Microscopy, Springer-Verlag, New York, pp. 75-77, 1985.

4) T. S. Rao-Sahib and D. B. Wittry, "X-ray continuum from thick elemental targets for 10-50 keV electrons," J. Appl. Phys., Vol 45(11), pp 5060-5068, Nov. 1974.

5) H. A. Bethe, "Zur Theorie des Durchgangs schneller Korpuskularstrahlen durch Materie," Ann. Phys. 5(5), pp 325-400, 1930.

6) R. Browning, T. Eimori, E. P. Traut, B. Chui, and R. F. W. Pease, "An elastic cross section model for use with Monte Carlo simulations of low energy electron scattering from high atomic number targets," J. Vac. Sci. Technol. B, Vol. 9(6), pp. 3578-3581, Nov. 1991.

7) L. Reimer and B. Lodding, "Calculation and Tabulation of Mott Cross-Sections for Large-Angle Electron Scattering," Scanning, Vol. 6(3), pp. 128-151, 1984.

8) Z. Czyzewski, D. MacCallum, A. Romig, and D. Joy, "Calculations of Mott scattering cross section, J. Appl. Phys., Vol. 68(7), pp. 3066-3072, Oct. 1990.

9) D. C. Joy and S. Luo, "An Empirical Stopping Power Relationship for Low-Energy Electrons," Scanning Vol. 11(4), pp. 176-180, 1989.

10) M. Gryzinski, "Classical theory of atomic collisions I. Theory of inelastic collisions, Phys. Rev., Vol. 138(2A), pp. 336-358, Apr. 1965.

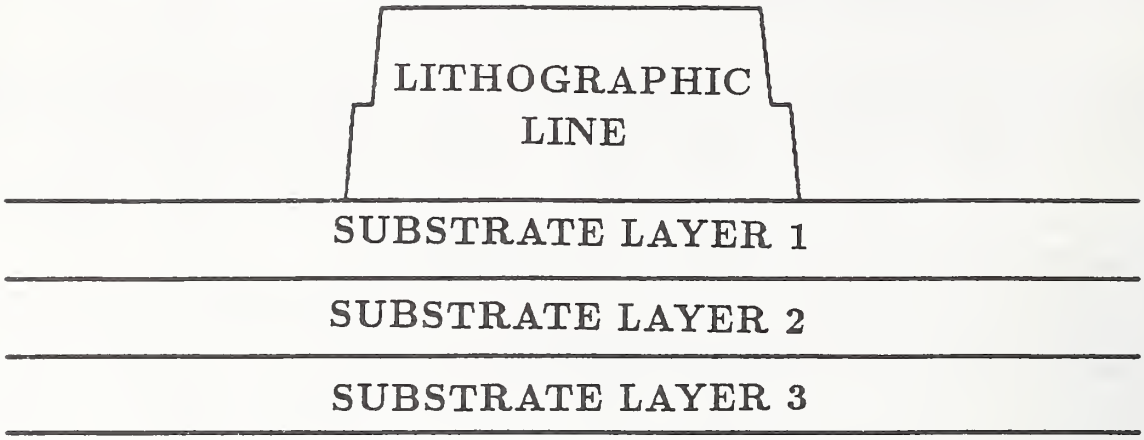

Fig. 1 Diagram of general specimen shape.

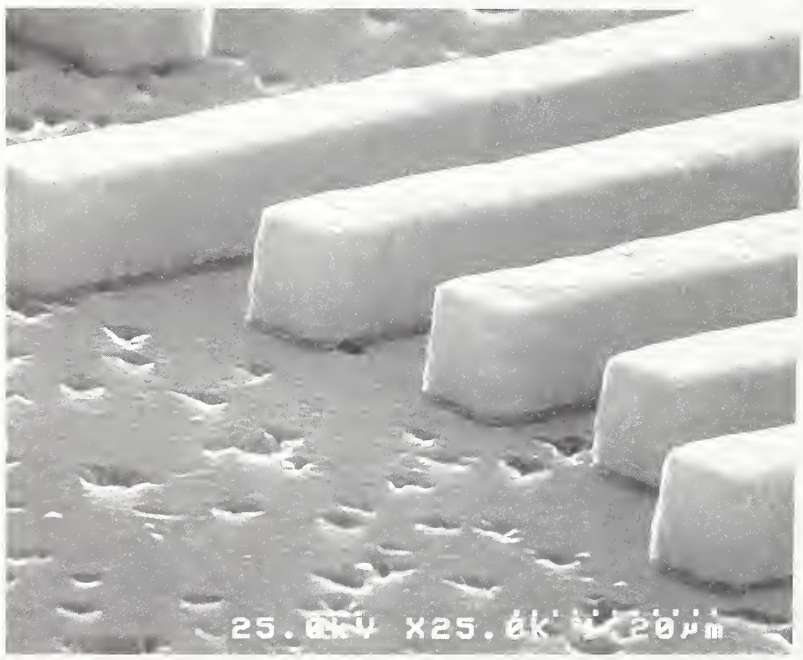

Fig. 2 SEM secondary image of lithographically produced gold lines on silicon substrate with chromium interlayer.

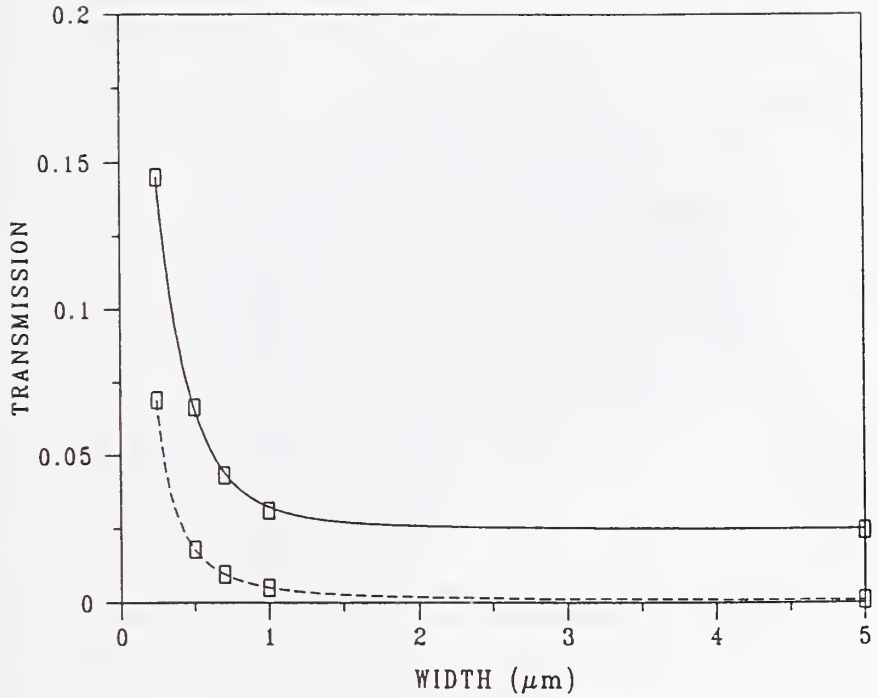

Fig. 3 Minimum transmission (i.e., at line center) through lines and substrate calculated as a function of linewidth. Squares are calculated values and lines are fits for total (solid) and detected (dash) transmission. The wall slope of the lines is 4 deg.

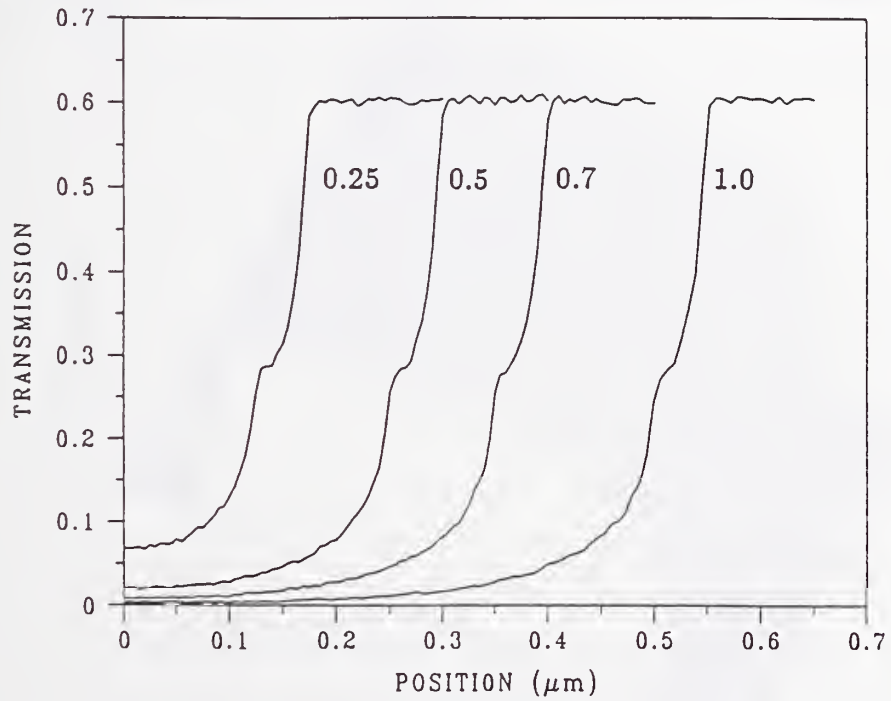

Fig. 4 Calculated detected transmission as a function of position across half of line for labeled linewidths in micrometers. The wall slopes are all 4 deg. Note "plateau-like" feature near the middle of each line edge.

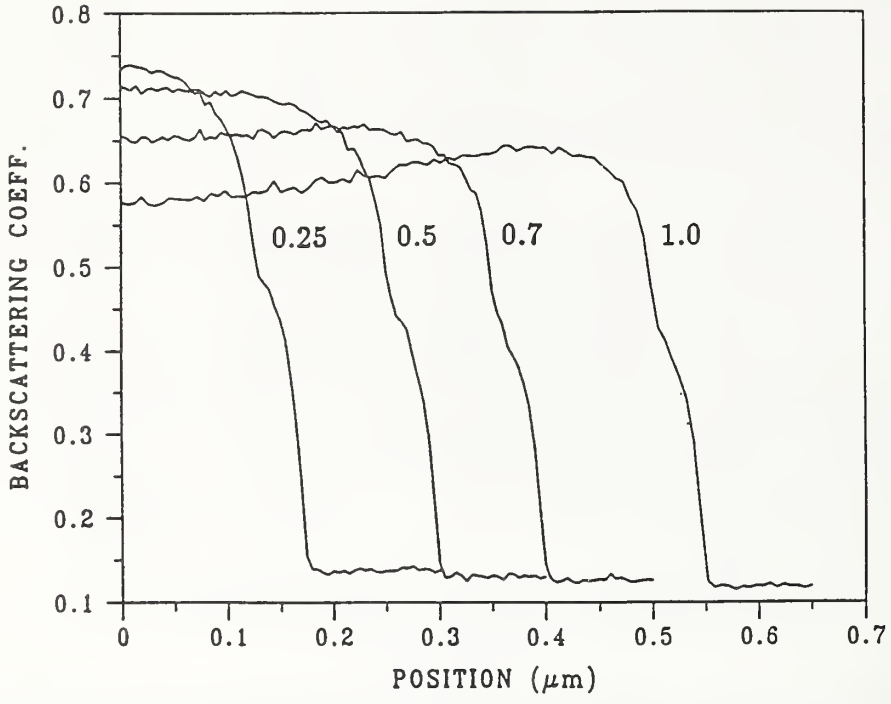

Fig. 5 Calculated backscattering coefficient for the same lines as in Fig. 4, again showing the "plateau-like" feature.

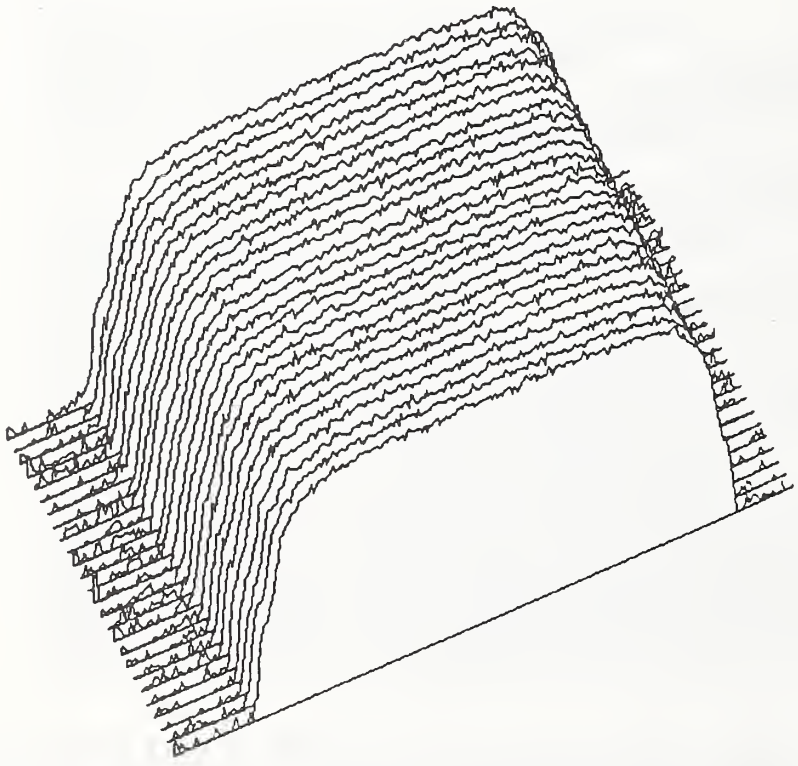

Fig. 6 Measured transmission along axis of gold line showing plateaus in the data near the middle of the edges.

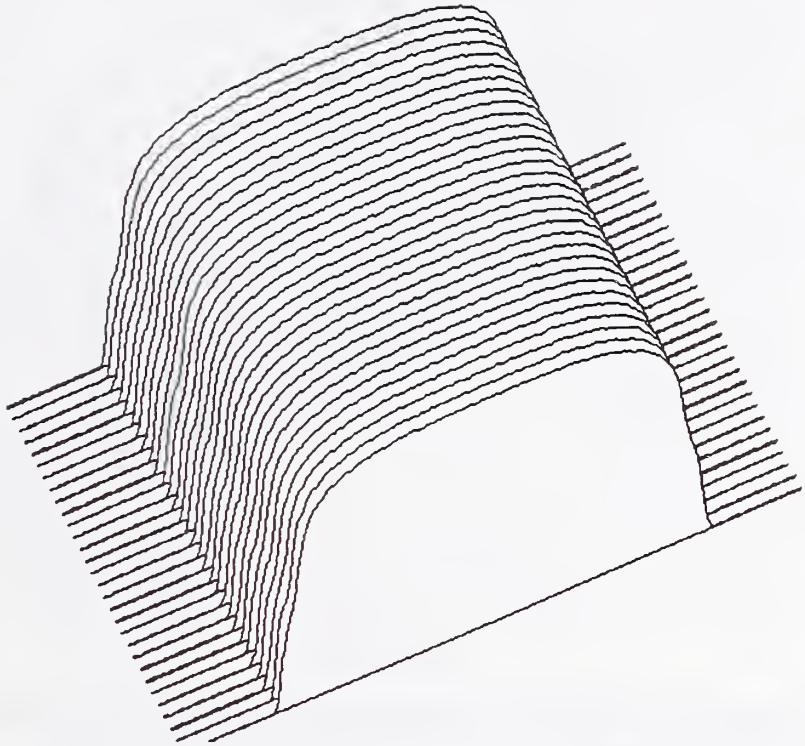

Fig. 7 Set of calculated lines for detected transmission along axis of gold line showing plateaus observed in data.

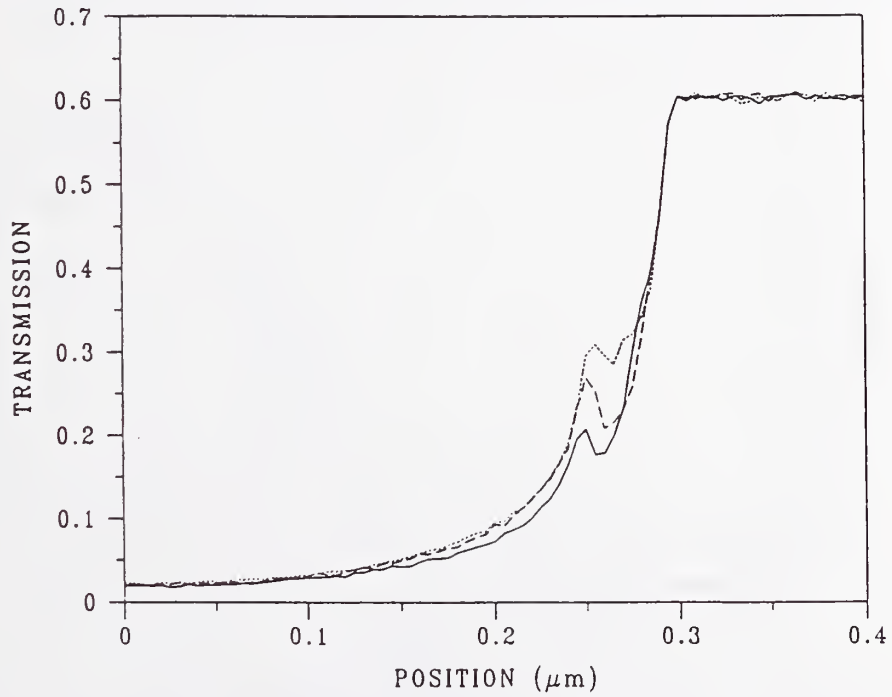

Fig. 8 Calculated detected transmission as a function of position along half of 0.5 μm wide lines with 2-deg wall slopes and a 20 nm jog 0.175 (short dash), 0.35 (long dash) and 0.525 (solid) μm above the bottom. Note serpentine structure as the beam crosses the jog region.

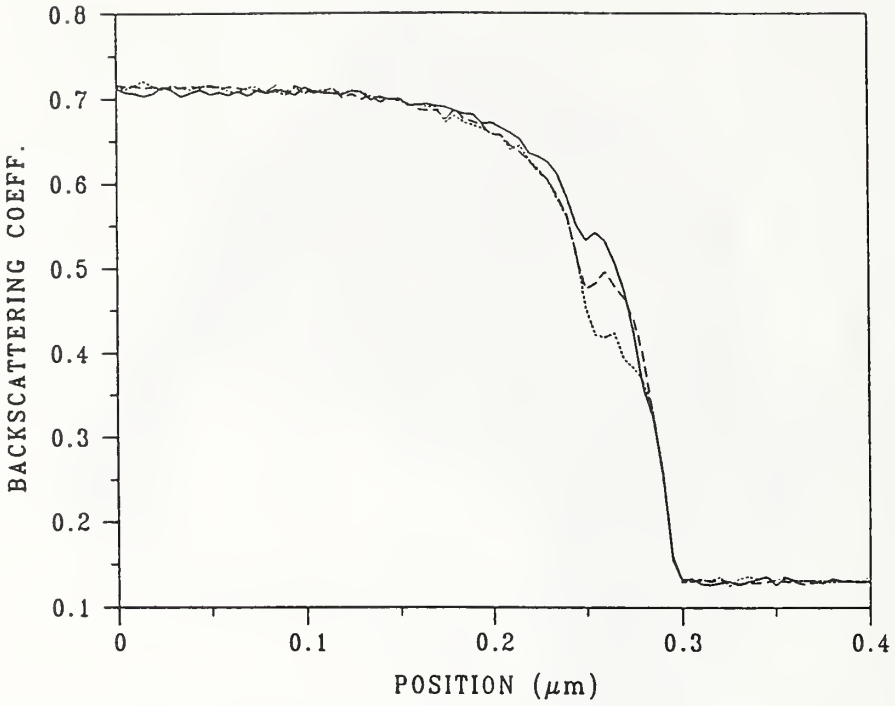

Fig. 9 Calculated backscattering coefficient as a function of position for the same lines as in Fig. 7 with the same line-font designations. The features associated with the jogs are similar to those in transmission.

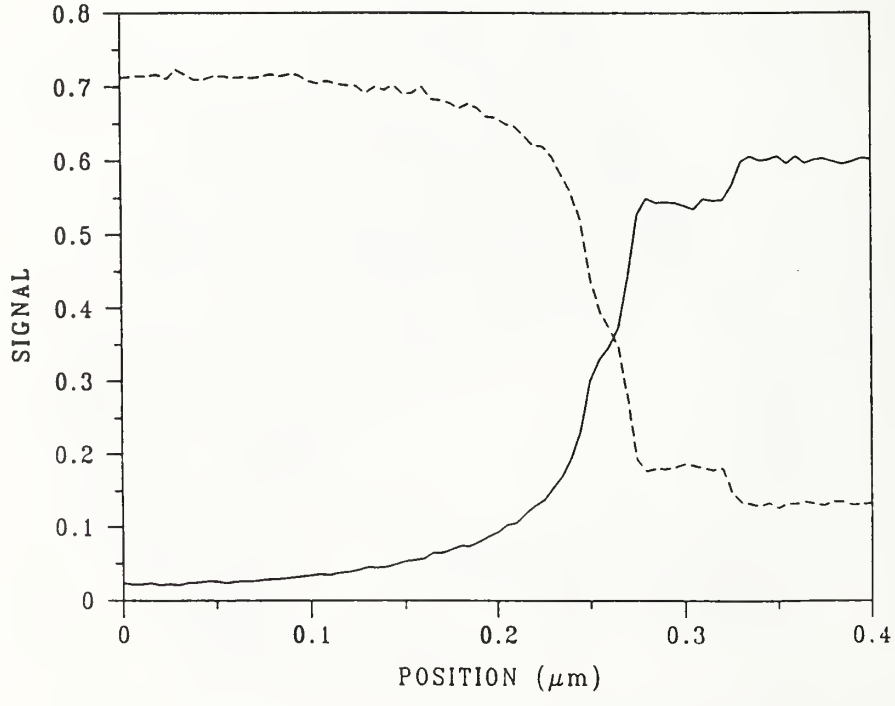

Fig. 10 Calculated transmission (solid) and backscattering coefficient (dash) for half of a 0.5 μm line with a 2-deg wall slope and a 50 nm foot 25 nm above the bottom.

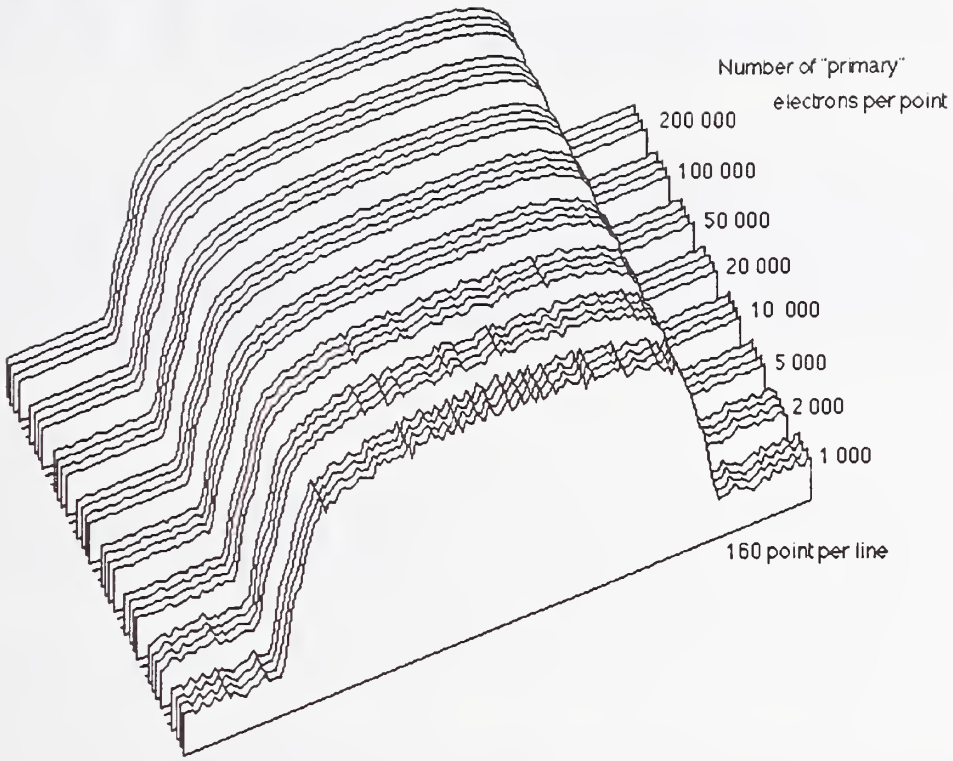

Fig. 11 Calculated detected transmitted signal across a 0.5 μm line with a 2-deg wall slope for between 1000 and 200000 electron trajectories per point and 160 points per line. Note how the noise level decreases with increasing number of trajectories.

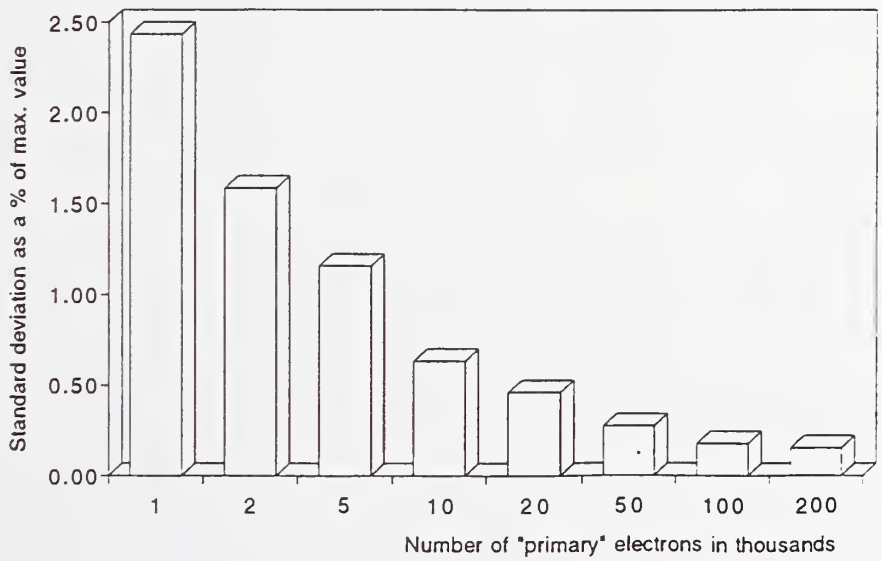

Fig. 12 Noise level (i.e., standard deviation as a percentage of maximum detected transmission) as a function of the number of trajectories.

NIST Technical Publications

Periodical

Journal of Research of the National Institute of Standards and Technology—Reports NIST research and development in those disciplines of the physical and engineering sciences in which the Institute is active. These include physics, chemistry, engineering, mathematics, and computer sciences. Papers cover a broad range of subjects, with major emphasis on measurement methodology and the basic technology underlying standardization. Also included from time to time are survey articles on topics closely related to the Institute's technical and scientific programs. Issued six times a year.

Nonperiodicals

Monographs—Major contributions to the technical literature on various subjects related to the Institute's scientific and technical activities.

Handbooks—Recommended codes of engineering and industrial practice (including safety codes) developed in cooperation with interested industries, professional organizations, and regulatory bodies.

Special Publications—Include proceedings of conferences sponsored by NIST, NIST annual reports, and other special publications appropriate to this grouping such as wall charts, pocket cards, and bibliographies.

Applied Mathematics Series—Mathematical tables, manuals, and studies of special interest to physicists, engineers, chemists, biologists, mathematicians, computer programmers, and others engaged in scientific and technical work.

National Standard Reference Data Series—Provides quantitative data on the physical and chemical properties of materials, compiled from the world's literature and critically evaluated. Developed under a worldwide program coordinated by NIST under the authority of the National Standard Data Act (Public Law 90-396). NOTE: The Journal of Physical and Chemical Reference Data (JPCRD) is published bimonthly for NIST by the American Chemical Society (ACS) and the American Institute of Physics (AIP). Subscriptions, reprints, and supplements are available from ACS, 1155 Sixteenth St., NW, Washington, DC 20056.

Building Science Series—Disseminates technical information developed at the Institute on building materials, components, systems, and whole structures. The series presents research results, test methods, and performance criteria related to the structural and environmental functions and the durability and safety characteristics of building elements and systems.

Technical Notes—Studies or reports which are complete in themselves but restrictive in their treatment of a subject. Analogous to monographs but not so comprehensive in scope or definitive in treatment of the subject area. Often serve as a vehicle for final reports of work performed at NIST under the sponsorship of other government agencies.

Voluntary Product Standards—Developed under procedures published by the Department of Commerce in Part 10, Title 15, of the Code of Federal Regulations. The standards establish nationally recognized requirements for products, and provide all concerned interests with a basis for common understanding of the characteristics of the products. NIST administers this program in support of the efforts of private-sector standardizing organizations.

Consumer Information Series—Practical information, based on NIST research and experience, covering areas of interest to the consumer. Easily understandable language and illustrations provide useful background knowledge for shopping in today's technological marketplace.

Order the **above** *NIST publications from: Superintendent of Documents, Government Printing Office, Washington, DC 20402.*

Order the **following** *NIST publications—FIPS and NISTIRs—from the National Technical Information Service, Springfield, VA 22161.*

Federal Information Processing Standards Publications (FIPS PUB)—Publications in this series collectively constitute the Federal Information Processing Standards Register. The Register serves as the official source of information in the Federal Government regarding standards issued by NIST pursuant to the Federal Property and Administrative Services Act of 1949 as amended, Public Law 89-306 (79 Stat. 1127), and as implemented by Executive Order 11717 (38 FR 12315, dated May 11, 1973) and Part 6 of Title 15 CFR (Code of Federal Regulations).

NIST Interagency Reports (NISTIR)—A special series of interim or final reports on work performed by NIST for outside sponsors (both government and non-government). In general, initial distribution is handled by the sponsor; public distribution is by the National Technical Information Service, Springfield, VA 22161, in paper copy or microfiche form.

U.S. Department of Commerce
National Institute of Standards and Technology
Gaithersburg, MD 20899-0001